Journal of Materials Chemistry

Cite this: J. Mater. Chem., 2012, 22, 4631

www.rsc.org/materials

COMMUNICATION

Enhanced n-type thermopower in distortion-free $LiMn_2O_4$

Taylor D. Sparks,*[a] Aleksander Gurlo[b] and David R. Clarke[a]

Received 1st December 2011, Accepted 2nd February 2012
DOI: 10.1039/c2jm16297k

A large n-type thermopower of −73 μV K^{-1} was observed at high temperatures (1100 K) for the first time in the mixed valence (Mn^{3+}/Mn^{4+}) spinel oxide $LiMn_2O_4$. The absence of a Jahn–Teller distortion leads to an electronic degeneracy ratio of 10/4 rather than 5/4 in the Heikes formula for the spin degeneracy contribution to the thermopower.

1. Introduction

Thermoelectric devices for power generation and solid-state refrigeration represent an important technology that could potentially offer long term solid-state solutions for increased energy efficiency and address environmental concerns. However, the efficiency of existing thermoelectric materials, limited temperature stability and potential scarcity of key elements, such as Te, have motivated researchers to consider oxides as thermoelectric materials.

Traditional thermoelectric materials such as Si, Bi_2Te_3 and Sb_2Te_3 achieve large ZT values by adjusting carrier density to compromise between electrical conductivity and thermopower. Typically the carrier density is ~10^{18}–10^{19} cm^{-3} with electrical conductivity of ~10^5 S m^{-1} and thermopower of ~200–300 μV K^{-1}. Some of the most recent advances in the field of thermopower generation rely on such conventional materials.[1–3]

The most promising oxide thermoelectrics are layered cobaltates, $Na_xCo_2O_4$. These exhibit metallic conductivity as well as an unusually large thermopower considering the high carrier density, ~10^{22} cm^{-3} (Seebeck coefficient, $Q_{300\ K}$ = 100 μV K^{-1} increasing to over 200 μV K^{-1} at 800 K). In fact, at high temperatures ZT > 1 has been achieved in layered cobaltates making them comparable to the best conventional materials.[4] The uncommonly large thermopower for a material with large carrier concentration has been attributed to the additional entropy arising from the spin and orbital degrees of freedom in Co^{3+} and Co^{4+} ions.[5] For strongly correlated systems, such as $Na_xCo_2O_4$, the Hubbard model expression for the Seebeck coefficient Q reduces to the Heikes formula:

$$Q = \frac{-k_B}{e}\ln\left(\frac{g_e}{g_h}\frac{x_h}{1-x_h}\right) \quad (1)$$

where k_B is the Boltzmann constant, e is the elementary positive charge, g_e and g_h are the electronic degeneracy terms of electron donors (Co^{3+}) and electron acceptors (holes, Co^{4+}), respectively, and x_h is the fraction of electron acceptors (Co^{4+}).[6]

Subsequently,[5] Koshibae *et al.* modified the Heikes formula to include the degeneracy of both ions involved in small polaron conduction and this formula has been applied to a variety of compounds in order to identify new potential thermoelectric oxides. Examples include $NaCo_2O_4$[5] and its derivative structures, $La_{1-x}Sr_xCoO_3$,[7] layered rhodium oxides $(Bi_{1-x}Pb_x)_{1.8}Sr_2Rh_{1.6}O_y$,[8] La,Mn,Cr-doped $SrRuO_3$,[9] $La_{1-x}Sr_xVO_3$,[10] manganese perovskites $Pr_{0.5}Ca_{0.5}MnO_3$ and double-perovskites $Ca(Mn_{3-y}Cu_y)Mn_4O_{12}$,[11] iron based structures $SrFeO_x$,[12] and $RBaCo_2O_{5+x}$ (R = Gd, Nd).[13] Demonstrating the application of the spin degeneracy methodology, shown in eqn (1), to a wider range of oxides has been identified as essential to the discovery of new thermoelectrics.[14]

In this work, we have re-investigated a strongly correlated compound, $LiMn_2O_4$, containing Mn^{3+} and Mn^{4+} ions in an octahedral crystal field (Table 1). Previous studies have demonstrated that large thermopower could be achieved in manganates through carrier doping.[15,16] However, Kobayashi *et al.* suggested that below 1000 K Jahn–Teller distortions in a variety of manganese perovskites containing an equal fraction of octahedrally coordinated Mn^{3+}/Mn^{4+} ions lead to an electron degeneracy ratio g_e/g_h = 5/4 corresponding to a small n-type thermopower of −20 μV K^{-1}.[11] In that work, thermal

Table 1 Electronic (g), spin (g_{spin}) and orbital ($g_{orbital}$) degeneracy for high spin (HS) Mn^{n+} (n = 2, 3, and 4) cations in tetrahedral (T), octahedral (O) and tetragonally (Jahn–Teller) distorted octahedral (t-O) crystal fields (CF)

Cation	d^n	CF	g_{spin}[a]	$g_{orbital}$[b]	g
Mn^{2+}	d^5	T	6	1	6
		O	6	3	18
Mn^{3+}	d^4	T	5	3	15
		O	5	2	10
		t-O	5	1	5
Mn^{4+}	d^3	T	4	3	12
		O	4	1	4

[a] Spin degeneracy: $g_{spin} = 2S + 1$, where S is the spin. [b] Total orbital degeneracy is calculated as a product of orbital degeneracies for each orbital type (t_{2g}, e_g, …): $g_{orbital} = \prod \frac{(n_{orbital})!}{(n_{orbital}-n_e)!n_e!}$, where $n_{orbitals}$ is the number of orbitals of one type and n_e denotes the number of unpaired electrons on this specific orbital type.

[a]*School of Engineering and Applied Sciences, Harvard University, Cambridge, MA, 02138, USA. E-mail: sparks@seas.harvard.edu; Fax: +01 (617)496 5333; Tel: +01 (617)495 6304*
[b]*Fachbereich Material- und Geowissenschaften, Technische Universität Darmstadt, Darmstadt, Germany*

energy possibly activated the degeneracy of the e_g orbital (g_e/g_h = 10/4, see Table 1) at high temperatures and although the thermopower increased slightly to -32 μV K^{-1} it did not reach the predicted value of -79 μV K^{-1} given by the Heikes formula.

In selecting candidate oxides with different Mn^{3+}/Mn^{4+} ratios to control the electron degeneracy term and enhance thermopower, we turned to the closely related field of mixed valence oxides as cathode materials for lithium ion batteries. In that body of work, a number of lithium manganese spinels have been identified that have both large electrical conductivities and behave as small polaron conductors due to electron hopping between the two oxidation states of manganese cations on octahedral (B, 16d) sites. This allows for variations of the mean oxidation state of manganese which, in turn, can be expected to influence the thermopower, see eqn (1). For example, $LiMn_2O_4$ ($[Li]^A[Mn^{3+},Mn^{4+}]^BO_4$), the simplest representative of Li–Mn–O spinels, has been widely studied as a cathode material, and features an equal amount ($x_h = 0.5$) of Mn^{3+} and Mn^{4+} on the octahedral site.

The low temperature thermopower of $LiMn_2O_4$ as a function of stoichiometry has been examined,[17] but only one study has investigated the thermopower of $LiMn_2O_4$ at elevated temperatures, close to where the Heikes formula is expected to be valid.[18] Curiously, this compound seemed to approach the high temperature spin degeneracy ratio of 5/4 (which corresponds to a thermopower of -20 μV K^{-1}) rather than 10/4 (which corresponds to -79 μV K^{-1}) despite the fact that $LiMn_2O_4$ is well understood to exhibit tetragonal symmetry below 280 K (tetragonal $LiMn_2O_4$, $I4_1/amd$).[19] The apparent inconsistency motivated us to re-examine this compound and clarify the role of Jahn–Teller distortion, using high temperature X-ray diffraction, between the crystal structure of $LiMn_2O_4$ and thermopower measurements.

2. Experimental

2.1 Synthesis and processing

Li–Mn–O spinel powders were synthesized at 1073 K (air, 6 h) from oxalates ($Li_2C_2O_4$ and $MnC_2O_4 \times 2H_2O$, Alfa Aesar) ground in appropriate ratio to achieve the final Li/Mn ratio equal to that in $LiMn_2O_4$. Then, rectangular bars (approximately $8 \times 2 \times 1$ mm^3 in dimension) for thermoelectric measurements were cut from Li–Mn–O pellets approximately 2 mm thick formed in ½ inch mold at 6 ton load for 60 s from the as-synthesized Li–Mn–O spinel phase powders and then sintered at 1073 K for 24 h in air.

2.2 X-ray diffraction & structural refinement

Room temperature and *in situ* high-temperature X-ray diffraction (XRD) data was collected using a Philips PANalytical X'Pert Pro diffractometer (Almelo, the Netherlands) in continuous-scanning mode at 45 kV 40 mA with a vertical θ–θ scanning geometry from 15° to 120° with a step size of 0.017° and a rate of 1.25 s/step. Fixed divergence and scattering slits of 0.5° and 0.02 radian Soller slits were used. The height of the sample in the furnace was zeroed by splitting the beam and the tilt was corrected by rocking the sample. Nickel filtered Cu-Kα radiation and a germanium detector were used with an Anton-Paar HTK1200N furnace to heat the samples for high-temperature data collection. The temperature fluctuation within the furnace was less than 1 K and the sample was heated slowly at 5 K min^{-1} and allowed 30 min to equilibrate before each scan was performed. Measurements were carried out in an air atmosphere at 298 K, 773 K, 873 K, 973 K, 1073 K, 1123 K with an additional scan of the sample after cooling again to 298 K.

Structural refinement was performed using the full-pattern Rietveld method based on least-squares refinement in the GSAS software. The background was fitted using a 6th order polynomial and a standard type 2 shape function (pseudo Voigt) was used for the profile to describe the shape of the peaks. The profile relies on the variables, U, V and W to describe the peak breadth (full width half maximum intensity, FWHM) as in $[U\tan^2(\theta) + V\tan(\theta) + W]^{1/2}$. Additionally, variables describing sample displacement, asymmetry, Lorentzian strain broadening, scale, lattice parameter, thermal displacement parameter, occupancy and atomic positional parameter were incorporated into the refinement. In total there were 19 variables refined simultaneously until convergence was achieved. The starting models were taken from Ishikawa[20] *et al.* (ICSD code 85400) and Wills[21] *et al.* (ICSD code 87775). Total compositional stoichiometry was constrained to be constant ($LiMn_2O_4$) by fixing the shift in fractional occupancy of Mn (B site) = $-$Li (B site) = -2 Mn (A site) = 2 Li (A site). Small corrections due to anomalous scattering factors, f′ and f″, for lithium, manganese and oxygen with Cu-Kα radiation were determined using FPRIME software. The spinel structural model with the origin on inversion center (-3m) at octahedral vacancy ($-1/8$, $-1/8$, $-1/8$) was applied. This model implies that the oxygen fraction coordinate u(ideal) = 1/4 = 0.250 (compare to u(ideal) = 3/8 = 0.375 for the structural model with the origin at A-site cation, 1/8, 1/8, 1/8) was applied for the refinement.[22]

2.3 Electrical transport measurements

Thermopower (Q) and electrical conductivity (σ) were simultaneously measured using an Ulvac ZEM-3 instrument (Methuen, MA). Samples approximately ($8 \times 2 \times 1$) mm^3 in dimension were cut from sintered pellets and polished to have orthogonal faces before being heated in air to 1273 K where measurements were made with $\Delta T = 20$ K, 30 K and 40 K using thermocouple probes ~3 mm apart. Measurements were made with decreasing temperature until the electrical resistivity was too large for further measurements to be made. Typically thermopower measurements done using a ZEM-3 system are accurate to approximate 10–15%. Measurements were taken on five separately prepared $LiMn_2O_4$ samples with less than 10% standard deviation. Furthermore, the ZEM-3 measurements of a constantan alloy standard were in good agreement with standard values over the whole temperature range measured.

2.4 Thermal transport measurements

Thermal conductivity (κ) was calculated using the standard relation

$$\kappa = \rho\alpha C_p \quad (2)$$

where ρ is density, α is the thermal diffusivity and C_p is the specific heat. Thermal diffusivity was measured *via* the laser flash method using the Clarke and Taylor model[23] on a Netzsch 457 (Netzsch, Selb, Germany). Samples were pellet shaped 10 mm in diameter and 1–2 mm in thickness. To reduce radiative transport the samples were sputter coated with a thin layer of gold and emissivity/absorption was promoted by spray coating with a thin layer of colloidal graphite. Samples were measured in a pure argon atmosphere and measurements were taken at 100 °C intervals up to 800 °C with a standard variation of less than 5%. The density of the samples was determined

by the Archimedes method using deionized water as an immersion medium (>90% dense). The heat capacity was calculated from the constituent oxides (Mn_2O_3, MnO_2 and Li_2O) using the Neumann-Kopp rule, known to be accurate to 5%. Finally, the thermal conductivity had a slight correction for remaining porosity using the Maxwell relation

$$\kappa' \Big/ \kappa = 1 - \frac{3}{2}\Phi \quad (3)$$

where κ' is the corrected porosity and ϕ is the sample porosity.

2.5 Scanning electron microscopy

The microstructure of $LiMn_2O_4$ compounds was investigated using scanning electron microscopy (SEM). Cross-sections of the material were polished and coated with a thin conductive metal layer (gold) before being imaged with a ZEISS EVO 55 scanning electron microscope (Oberkochen, Germany). Images were obtained *via* secondary electrons with a working distance of ~9 mm, a variety of magnifications, and 15.75 kV accelerating voltage.

3. Results and discussion

3.1 Phase composition and structural refinement

The results of the *in situ* heating X-ray diffraction confirmed that in the air-sintered samples the major phase is an undistorted, cubic spinel-type $LiMn_2O_4$ (Fd-3m, a = 8.2514 Å, Z = 8). At room temperature, there was only 1.5 wt% of the tetragonal phase ($I4_1$/amd, a = 5.82 Å, c = 8.315 Å, Z = 4) and no appreciable amount at elevated temperatures (Table 2, Fig. 1). The finding of a cubic spinel extends the work of Yamada *et al.* who showed that full transition to the tetragonal phase ($I4_1$/amd) only occurs below 280 K.[19]

The Rietveld refinement of room temperature XRD data is presented in Fig. 1 with an inset showing elevated temperature data (Table 2 has detailed results for all temperatures). With increasing temperature the XRD patterns visibly changed (see inset in Fig. 1) in two ways: (1) the peaks shifted to smaller 2θ values as thermal expansion caused the unit cell volume to increase and (2) the peak widths decreased and the distinction between Cu-Kα_1 and Cu-Kα_2 increased. The peak widths are greatest at room temperature because of the presence of the tetragonal phase. The convolutions for additional peaks from the lower symmetry $I4_1$/amd phase produce wider peaks. Although the weight fraction of the tetragonal phase refined to zero for all non-ambient temperatures, the width of the peaks at high temperatures do seem to very slightly, yet systematically decrease

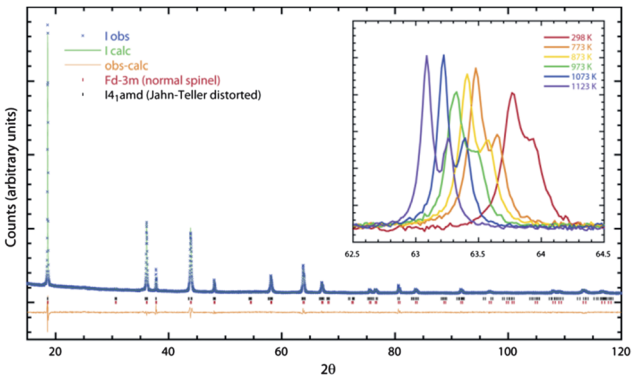

Fig. 1 X-Ray diffraction pattern and Rietveld refinement results for $LiMn_2O_4$ at 298 K. The weighted residual, R_{wp}, for the refinement was 3.46% and the fraction of the undistorted spinel $LiMn_2O_4$ phase (Fd-3m) was 98.5 wt% with only 1.5 wt% tetragonal ($I4_1$/amd) $LiMn_2O_4$ phase. The inset shows the XRD pattern of the (440) reflection for the Fd-3m phase for different temperatures. The lattice parameter clearly increases evidenced by the peak shifting to smaller 2θ values. Also, the 298 K peak is considerably wider than the others because the lower symmetry tetragonal phase includes convolutions of two additional reflections; (224) at 63.5° and (440) at 63.9°.

indicating that perhaps there is a very small amount of tetragonal phase remaining that is not being accounted for in the Rietveld refinement.

No evidence of secondary phases was observed in SEM images (see Fig. 2). The material appeared homogenous with uniform micron scale porosity in general agreement with there being <10% porosity as measured *via* the Archimedes method.

The coefficient of thermal expansion (CTE) is calculated to be 93–120 ppm/K over the range 298–1123 K based on the increase in the lattice parameter for the $LiMn_2O_4$ Fd-3m phase. The compound also underwent slight inversion upon heating, that is to say, a fraction of Li^+ ions occupied the octahedral B (16d) site instead of the tetrahedral A (8a) site and Mn ions did the opposite (Fig. 3). At room temperature only 2.5% of the B site ions were Li^+ but by 1123 K the percentage had increased to 8.1%. The inversion can likely be ascribed to strain minimization as the larger Li^+ ions (ionic radius 73/90 pm for tetrahedral and octahedral coordination respectively) increase their coordination from 4 to 6. The smaller manganese ions (ionic radius 64/78.5 and 53/67 pm for high spin Mn^{3+} and Mn^{4+} in tetrahedral and octahedral coordination, respectively) decrease coordination. The ionic radius for Mn^{3+} in tetrahedral coordination is not available in the literature but was calculated from the average

Table 2 Structure refinement details for $LiMn_2O_4$ measured in air as a function of temperature (standard deviations in shift shown beneath in parentheses)

T/K	a (Fd-3m), Å	u[a]	%Li A site, *y*	%Mn B site	R_{wp}%	wt% $I4_1$/amd
298 (first)	8.2513(7)	0.26195 (20)	94.7 (6)	97.3 (3)	3.46	1.5
773	8.2935(8)	0.26275 (20)	89.1 (7)	94.6 (3)	3.21	—
873	8.3047(8)	0.26271 (20)	87.3 (7)	93.7 (4)	3.21	—
973	8.3184(8)	0.26333 (20)	83.4 (7)	91.7 (4)	3.05	—
1073	8.3319(7)	0.26263 (20)	84.4 (7)	92.2 (3)	3.22	—
1123	8.3495(7)	0.26168 (20)	83.7 (6)	91.9 (3)	3.27	—
298 (last)	8.2520(7)	0.26177 (20)	95.2 (7)	97.6 (3)	3.22	—

[a] Oxygen fractional coordinate, origin at inversion center (−3m) at octahedral vacancy (−1/8, −1/8, −1/8).

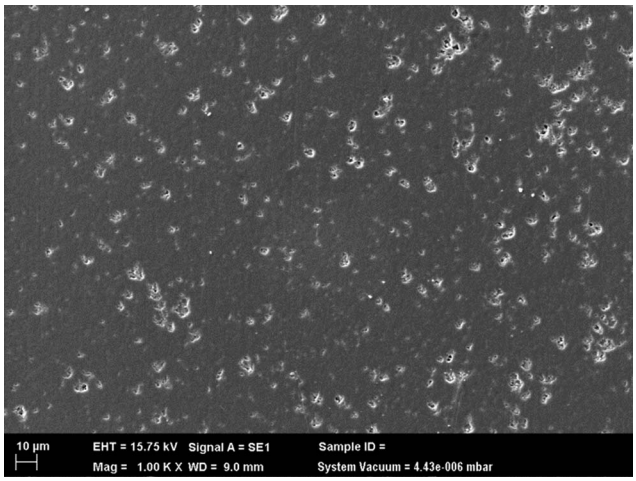

Fig. 2 Scanning electron microscope image of the $LiMn_2O_4$ microstructure. Uniform micron scale porosity (<10%) exists throughout the material but there is no evidence of any additional phases.

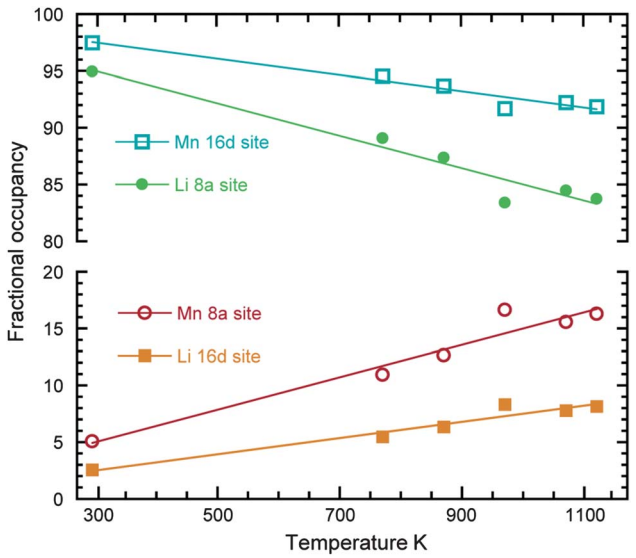

Fig. 3 Fraction of the A (tetrahedral) and B (octahedral) sites in the $LiMn_2O_4$ spinel occupied by Li and Mn ions plotted against temperature. The lines represent linear best fits ($R^2 = 0.971$). Inversion on the B site is observed to increase linearly over the temperature range.

bond length $d(Mn^{3+}{}_{tetr}–O^{2-}) = 188(1)$ pm in spinels[24] taking the radius of O^{2-} as 124 pm.

Inversion of the $LiMn_2O_4$ structure with increasing temperature has not been reported previously. However, we find that the structure of $LiMn_2O_4$ is sensitive to cooling/heating conditions and can undergo complex phase transformations and cation rearrangement since the amount of lithium, manganese and oxygen is freely adjustable and the mean Mn oxidation state is not fixed.[25]

At the time of writing we do not have any independent experimental data confirming the occupancies of tetrahedral and octahedral sites by Mn^{3+} and Mn^{4+} ions. Instead, we estimated possible occupancies by comparing experimental (u = 0.26195/0.26168 at 298 and 1073 K, respectively) and calculated oxygen fractional coordinate (u) for $LiMn_2O_4$ employing different distortion models, *i.e.* occupancies of A-sites by (i) equal amount of Mn^{3+} and Mn^{4+} cations in $[Li_{1-i}{}^{+}Mn_{i/2}{}^{3+}Mn_{i/2}{}^{4+}]^{A}[Li_{i}{}^{+}Mn_{1-i/2}{}^{3+}Mn_{1-i/2}{}^{4+}]^{B}O_4$ (u = 0.26223/0.26133), (ii) only by Mn^{3+} cations in $[Li_{1-i}{}^{+}Mn_{i}{}^{3+}]^{A}[Li_{i}{}^{+}Mn_{1-i}{}^{3+}Mn_{1}{}^{4+}]^{B}O_4$ and (u = 0.26240/0.26183), (iii) only by Mn^{4+} cations in $[Li_{1-i}{}^{+}Mn_{i}{}^{4+}]^{A}[Li_{i}{}^{+}Mn_{1}{}^{3+}Mn_{1-i}{}^{4+}]^{B}O_4$ (u = 0.26207/0.26084) and (iv) that in undistorted $[Li^{+}]^{A}[Mn^{3+}Mn^{4+}]^{B}O_4$ spinel (u = 0.26269). The oxygen fractional coordinate (u) was calculated according to eqn (2)–(5)[22] using the experimentally determined fractional occupancy (i) of Li^+ on A sites ($i = 0.01y$, see Table 2):

$$u = 0.25 + \left\{0.375 - \left(0.3876\left(\frac{\langle r(B)\rangle}{\langle r(A)\rangle}\right)^{0.07054}\right)\right\} \quad (4)$$

$$\langle r(A)\rangle = i^{A}_{Li} r_{tetr}(Li) + (1 - i^{A}_{Li})\, r_{tetr}(Mn^{3+/4+}) \quad (5)$$

$$\langle r(B)\rangle = 0.5 i^{B}_{Li} r_{oct}(Li) + (1 - i^{B}_{Li})\, r_{oct}(Mn^{3+/4+}) \quad (6)$$

As the distortion of the spinel structure is small, the comparison between experimental and calculated structural parameters given above does not provide unambiguous evidence for preferential site occupancies. Nevertheless, our assessment is that the fraction of octahedral Mn^{4+} lies in the range between 0.46 and 0.54 at 1073 K. Furthermore, as we have found that the lattice parameter of the cubic $LiMn_2O_4$ increases with temperature, we can exclude the possibility of an increase in mean oxidation state of manganese (for this, an opposite effect will be observed, see ref. 25). According to TGA data,[26] at T > 1053 K $LiMn_2O_4$ loses oxygen becoming non-stoichiometric.[25] This is not the case for our study. Since we also did not observe the decomposition of $LiMn_2O_4$ which typically happens at T > 1113 K (XRD) upon heating in air,[26] we can exclude the formation of delithiated and manganese-deficient spinels.

Summarizing, our *in situ* heating XRD characterization has unambiguously demonstrated that: (i) single-phase undistorted normal $LiMn_2O_4$ spinel is stable over a broad temperature range (298–1123 K) and, (ii) the inversion of spinel structure is less than 8% even at the highest temperature studied (1123 K). Therefore, as $LiMn_2O_4$ is free of a Jahn–Teller distortion it provides a model to ascertain the contribution of the electron degeneracy term to the thermopower of Mn^{3+}/Mn^{4+} compounds.

3.2 Electrical and thermal conductivity

The temperature dependence of the electrical conductivity is consistent with previous measurements on $LiMn_2O_4$. For example, Fig. 4 shows the electrical resistivity approaching a minimum value of 9 mΩ cm, comparable to the high temperature Ioffe-Regel limit of 2 mΩ cm.[11] The activation energy (E_A) for small polaron conduction was calculated to be 0.36 ± 0.01 eV by plotting $ln(\sigma T)$ against 1/T and setting the slope equal to $-E_A/k_B$ (see inset to Fig. 4). This value agrees well with the 0.4 eV reported experimentally for small-polaron conduction[11,18] in $LiMn_2O_4$. The thermal conductivity values ranging between 2 and 2.5 W m^{-1} K (see Table 3) are typical for an oxide lacking alloying or nanostructured defects to scatter phonons.

3.3. Seebeck coefficient

In contradiction to earlier thermopower reports for $LiMn_2O_4$[18] whose thermopower corresponds to Jahn–Teller distorted MnO_6 octahedra,

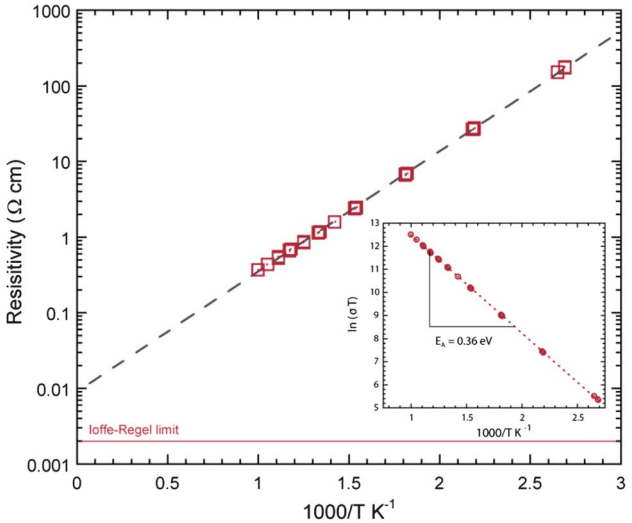

Fig. 4 Arrhenius plot of the electrical resistivity. The high temperature value of the $LiMn_2O_4$ series approaches (dashed line) 9 mΩ cm, close to the Ioffe-Regel limit (solid line) of 2 mΩ cm for a mean free electron path of 2.9 Å. The inset is an Arrhenius plot with an activation energy of 0.36 ± 0.01 eV, consistent with small polaron conduction.

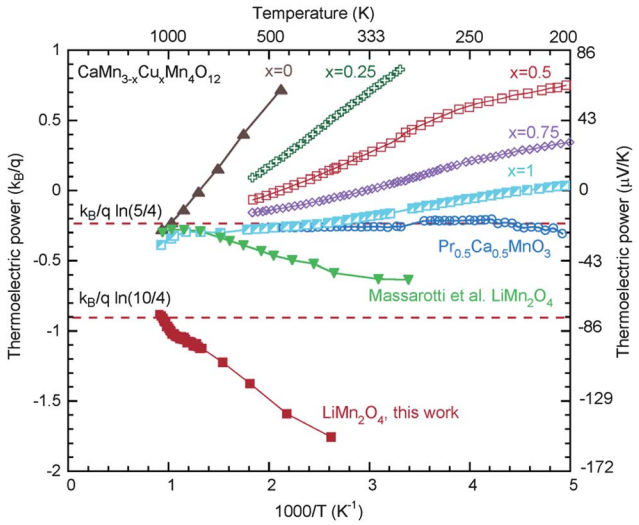

Fig. 5 Thermopower *versus* temperature for $LiMn_2O_4$ from this work compared with other Mn compounds as reported by Kobayashi *et al.*[11] The dashed lines at −20 and −79 μV K^{-1} represent the predictions based on the high temperature limit of the Heikes formula for Mn^{3+}/Mn^{4+} ions in equal concentration with and without a Jahn–Teller distortion (g_3/g_4 = 5/4 or 10/4). The measured values reach −73 μV K^{-1} in good agreement with the Heikes formula for an undistorted structure.

the thermopower measured in this work reaches a high temperature value of −73 μV K^{-1}. Interestingly, this value is more than 3 times larger than previously reported in small-polaron conducting manganates with equal Mn^{3+}/Mn^{4+} concentrations (Fig. 5). It is, however, fully consistent with the high temperature limit of the Heikes formula (see eqn (1) and Table 1) for small polaron conduction between undistorted octahedrally coordinated Mn^{3+} and Mn^{4+} ions.

In the following paragraphs we address the effect of inversion on thermopower. Koshibae *et al.* shows[27] that when multiple ion pairs are present (which differ either in oxidation state or coordination environment, for example, Mn^{3+}/Mn^{4+} on tetrahedral and octahedral sites) the total thermopower should simply be the weighted fraction of each pair's contribution:

$$Q = \frac{-k_B}{e}\left\{\ln\left(\frac{g_{i,c}}{g_{i,c}}\frac{x_c}{1-x_c}\right)\frac{c}{c+d} + \ln\left(\frac{g_{j,d}}{g_{j,d}}\frac{x_d}{1-x_d}\right)\frac{d}{c+d}\right\} \quad (7)$$

Here c and d are fractions of each ion pair, $g_{(i,j),(c,d)}$ is the electron degeneracy of the ion pairs (i,j) on sites (c,d) and $x_{(c,d)}$ is the fraction of Mn^{4+} on each site. Considering contributions only from Mn^{3+}/Mn^{4+} pairs and assuming their equal distribution between tetrahedral and octahedral sites ($x_c = x_d = 0.5$), we obtain for 1073 K

$$Q = \frac{-k_B}{e}\left\{0.06\ln\left(\frac{15}{12}\right) + 0.94\ln\left(\frac{10}{4}\right)\right\} \quad (8)$$

Evaluation of this expansion indicates only a slight reduction in thermopower from −79 to −75 μV K^{-1}.

Finally, the development of n-type oxide thermoelectrics with high ZT values requires large values for the power factor ($Q^2\sigma$). So, while we report an increase in the Seebeck coefficient, the power factor remains too low, ~10^{-6} W/mK^2, because the high electrical resistivity is unaffected. Nevertheless, the evidence that Mn^{3+}/Mn^{4+} ion mixtures in octahedral stereochemistry can be stabilized in a Jahn–Teller distortion-free compound is encouraging. The finding suggests that other oxides may exist as well where we can take advantage of the large entropy exchange and resultant spin degeneracy ratio to achieve large thermopowers. Future studies will explore new doping strategies on both A and B sites to enhance the electrical conductivity.

Table 3 Thermal conductivity of $LiMn_2O_4$ samples

T/K	400	500	600	700	800	900	1000
Thermal Conductivity/W m^{-1} K	2.0	2.1	2.3	2.4	2.4	2.4	2.3

4. Conclusions

$LiMn_2O_4$ samples with the cubic (Fd-3m) spinel structure exhibit a large n-type high temperature thermopower of −73 μV K^{-1}. This thermopower is enhanced relative to other mixed valence Mn^{3+}/Mn^{4+} compounds studied previously. The increase in thermopower can be understood as due to an absence of a Jahn–Teller distortion in cubic $LiMn_2O_4$. Relative to the structure with a Jahn–Teller distortion, the orbital degeneracy is doubled. As a result, the electronic degeneracy ratio g_e/g_h for the two ions involved in small-polaron conduction, Mn^{3+} & Mn^{4+}, is increased from 5/4 (Jahn–Teller distorted) to 10/4 (Jahn–Teller distortion free). Our experimental value at high temperature, −73 μV K^{-1}, is also consistent with the prediction of the thermopower from the Heikes formula (−79 μV K^{-1}) using this latter value of the electronic degeneracy.

Acknowledgements

The authors extend their gratitude to Dr Scott Speakman at the MIT Center for Materials Science and Engineering for technical assistance with *in situ* X-ray diffraction and helpful discussion. Funding sources: The support for A.G. by the Alexander-von-Humboldt Foundation is gratefully acknowledged. The research was performed at Harvard University through the Gordon McKay Endowment.

Notes and references

1 W. Choi, S. Hong, J. T. Abrahamson, J.-H. Han, C. Song, N. Nair, S. Baik and M. S. Strano, Chemically driven carbon-nanotube-guided thermopower waves, *Nat. Mater.*, 2010, **9**(5), 423.
2 S. Walia, R. Weber, K. Latham, P. Petersen, J. T. Abrahamson, M. S. Strano and K. Kalantar-zadeh, Oscillatory Thermopower Waves Based on Bi2Te3 Films, *Adv. Funct. Mater.*, 2011, **21**(11), 2072.
3 S. Walia, R. Weber, S. Sriram, M. Bhaskaran, K. Latham, S. Zhuiykov and K. Kalantar-zadeh, Sb2Te3 and Bi2Te3 based thermopower wave sources, *Energy Environ. Sci.*, 2011, **4**(9), 3558.
4 R. Funahashi, I. Matsubara, H. Ikuta, T. Takeuchi, U. Mizutani and S. Sodeoka, An Oxide Single Crystal with High Thermoelectric Performance in Air, *Jpn. J. Appl. Phys.*, 2000, **39**(Part 2, No. 11B), L1127–L29.
5 W. Koshibae, K. Tsutsui and S. Maekawa, Thermopower in cobalt oxides, *Phys. Rev. B: Condens. Matter*, 2000, **62**(11), 6869.
6 R. R. Heikes and R. W. Ure, *Thermoelectricity: science and engineering*. Interscience Publishers, 1961).
7 J. Androulakis, P. Migiakis and J. Giapintzakis, La0.95Sr0.05CoO3: An efficient room-temperature thermoelectric oxide, *Appl. Phys. Lett.*, 2004, **84**(7), 1099.
8 S. Okada and I. Terasaki, Physical Properties of Bi-Based Rhodium Oxides with RhO2 Hexagonal Layers, *Jpn. J. Appl. Phys.*, 2005, **44**(4A), 1834–37.
9 Y. Klein, S. Hébert, A. Maignan, S. Kolesnik, T. Maxwell and B. Dabrowski, Insensitivity of the band structure of substituted SrRuO3 as probed by Seebeck coefficient measurements, *Phys. Rev. B: Condens. Matter Mater. Phys.*, 2006, **73**(5), 052412.
10 M. Uchida, K. Oishi, M. Matsuo, W. Koshibae, Y. Onose, M. Mori, J. Fujioka, S. Miyasaka, S. Maekawa and Y. Tokura, Thermoelectric response in the incoherent transport region near Mott transition: The case study of La1-xSrxVO3, *Phys. Rev. B: Condens. Matter Mater. Phys.*, 2011, **83**(16), 165127.
11 W. Kobayashi, I. Terasaki, M. Mikami, R. Funahashi, T. Nomura and T. Katsufuji, Universal charge transport of the Mn oxides in the high temperature limit, *J. Appl. Phys.*, 2004, **95**(11), 6825–27.
12 G. V. M. Williams, E. K. Hemery and D. McCann, Magnetic and transport properties of SrFeOx, *Phys. Rev. B: Condens. Matter Mater. Phys.*, 2009, **79**(2), 024412.
13 A. A. Taskin, A. N. Lavrov and Y. Ando, Origin of the large thermoelectric power in oxygen-variable $RBaCo_2O_{5+x}$ (R = Gd, Nd), *Phys. Rev. B: Condens. Matter Mater. Phys.*, 2006, **73**(12), 121101.
14 S. Hebert and A. Maignan, Thermoelectric oxides. in *Functional Oxides*. Edited by Duncan W. Bruce, D. O'Hare, and R. I. Walton. Wiley-VCH, 2010.
15 J. Hejtmánek, Z. Jirák, M. Maryško, C. Martin, A. Maignan, M. Hervieu and B. Raveau, Interplay between transport, magnetic, and ordering phenomena in Sm1-xCaxMnO3, *Phys. Rev. B: Condens. Matter*, 1999, **60**(20), 14057.
16 Y. Wang, Y. Sui, H. Fan, X. Wang, Y. Su, W. Su and X. Liu, High Temperature Thermoelectric Response of Electron-Doped CaMnO3, *Chem. Mater.*, 2009, **21**(19), 4653.
17 J. Marzec, K. Świerczek, J. Przewoźnik, J. Molenda, D. R. Simon, E. M. Kelder and J. Schoonman, Conduction mechanism in operating a LiMn2O4 cathode, *Solid State Ionics*, 2002, **146**(3–4), 225.
18 V. Massarotti, D. Capsoni, M. Bini, G. Chiodelli, C. B. Azzoni, M. C. Mozzati and A. Paleari, Electric and Magnetic Properties of LiMn2O4- and Li2MnO3-Type Oxides, *J. Solid State Chem.*, 1997, **131**(1), 94.
19 A. Yamada and M. Tanaka, Jahn–Teller structural phase transition around 280 K in LiMn2O4, *Mater. Res. Bull.*, 1995, **30**(6), 715.
20 Y. Ishikawa and S. Higuchi, Structure Analysis of Some Li-Metal Double Oxides, *Journal of Tosoh Research*, 1997, **41**, 35–48.
21 A. S. Wills, N. P. Raju and J. E. Greedan, Low-temperature structure and magnetic properties of the spinel $LiMn_2O_4$: A frustrated antiferromagnet and cathode material, *Chem. Mater.*, 1999, **11**(6), 1510–18.
22 K. E. Sickafus, J. M. Wills and N. W. Grimes, Structure of spinel, *J. Am. Ceram. Soc.*, 1999, **82**(12), 3279–92.
23 L. M. Clark III and R. E. Taylor, Radiation loss in the flash method for thermal diffusivity, *J. Appl. Phys.*, 1975, **46**(2), 714.
24 F. Bosi, U. Halenius, G. B. Andreozzi, H. Skogby and S. Lucchesi, Structural refinement and crystal chemistry of Mn-doped spinel: A case for tetrahedrally coordinated Mn3+ in an oxygen-based structure, *Am. Mineral.*, 2007, **92**(1), 27–33.
25 J. M. Paulsen and J. R. Dahn, Phase diagram of Li–Mn–O spinel in air, *Chem. Mater.*, 1999, **11**(11), 3065–79.
26 M. M. Thackeray, M. F. Mansuetto, D. W. Dees and D. R. Vissers, The thermal stability of lithium-manganese-oxide spinel phases, *Mater. Res. Bull.*, 1996, **31**(2), 133–40.
27 V. Zlatić, A. C. Hewson, W. Koshibae, and S. Maekawa, Thermoelectric Effect in Transition Metal Oxides. pp. 69. in Properties and Applications of Thermoelectric Materials. *NATO Science for Peace and Security Series B: Physics and Biophysics*. Springer Netherlands, 2009.

